Sr-containing hydroxyapatite: morphologies of HA crystals and bioactivity on osteoblast cells

Sr-containing hydroxyapatite: morphologies of HA crystals and bioactivity on osteoblast cells

Valentina Aina[1†], Loredana Bergandi[2*†], Gigliola Lusvardi[3], Gianluca Malavasi[3], Flora E. Imrie[4], Iain R. Gibson[4], Giuseppina Cerrato[1], Dario Ghigo[2]

[1] Department of Chemistry, Università degli Studi di Torino, Via P. Giuria 7, 10125 Torino, Italy; Centre of Excellence NIS (Nanostructured Interfaces and Surfaces); INSTM (Italian National Consortium for Materials Science and Technology), UdR Università di Torino.

[2] Department of Genetics, Biology and Biochemistry, Università degli Studi di Torino, Via Santena 5/bis, 10126 Torino, Italy.

[3] Department of Chemistry, Università degli Studi di Modena e Reggio Emilia, Via Campi 183, 41100 Modena, Italy.

[4] School of Medical Sciences, Institute of Medical Sciences, University of Aberdeen, Foresterhill, Aberdeen, AB25 2ZD, United Kingdom.

[†] Valentina Aina and Loredana Bergandi contributed equally to this work

* to whom correspondence should be addressed:

Dr. Loredana Bergandi, E-mail address: loredana.bergandi@unito.it

Tel +39 011 6705843

Fax +39 011 6705845

Abstract

A series of Sr-substituted hydroxyapatites (HA), of general formula $Ca_{(10-x)}Sr_x(PO_4)_6(OH)_2$, where x = 2 and 4, were synthesized by solid state methods and characterized extensively. The reactivity of these materials in cell culture medium was evaluated and, the behaviour towards MG-63 osteoblast cells (in terms of cytotoxicity and proliferation assays) was studied. Future *in vivo* studies will give further insights into the behaviour of the materials.

A paper by Lagergren *et al.* (1975), concerning Sr-substituted HA prepared by a solid state method, reports that the presence of Sr in the apatite composition strongly influences the apatite diffraction patterns. Zeglinsky *et al.* (2012) investigated Sr-substituted HA by *ab initio* methods and Rietveld analyses and reported changes in the HA unit cell volume and shape due to the Sr addition.

To further clarify the role played by the addition of Sr on the physico-chemical properties of these materials we prepared Sr-substituted HA compositions by a solid state method, using different reagents, thermal treatments and a multi-technique approach. Our results indicated that the introduction of Sr at the levels considered here does influence the structure of HA. There is also evidence of a decrease in the crystallinity degree of the materials upon Sr addition. The introduction of increasing amounts of Sr into the HA composition causes a decrease in the specific surface area and an enrichment of Sr-apatite phase at the surface of the samples. Bioactivity tests show that the presence of Sr causes changes in particle size and/or morphology during soaking in MEM solution; on the contrary the morphology of pure HA does not change after 14 days of reaction. The presence of Sr, as Sr-substituted HA and $SrCl_2$, in cultures of human MG-63 osteoblasts did not produce any cytotoxic effect. In fact, Sr-substituted HA increased the proliferation of osteoblast cells and enhanced cell differentiation;: Sr in HA has a positive effect on MG-63 cells. In contrast, Sr ions alone, at the concentrations released by Sr-HA (1.21-3.24 ppm), influenced neither cell proliferation nor differentiation. Thus the positive effects of Sr in Sr-HA materials are probably due to the co-action of other ions such as Ca and P.

Keywords: Sr-substituted apatite; solid state synthesis; physico-chemical characterization, cytotoxicity; human MG-63 osteoblasts; LDH, lactate dehydrogenase; H3- thymidine; ALP, alkaline phosphatase.

1. Introduction

Hydroxyapatite (HA) is a calcium phosphate of formula $Ca_{10}(PO_4)_6(OH)_2$. Of all the calcium phosphate ceramics used as bone-replacement materials, HA most closely resembles the main inorganic phase of bone and teeth in humans. It is a very insoluble compound and, under physiological conditions of temperature and pH, is the most insoluble calcium phosphate [1]. The inorganic component of bone differs from stoichiometric HA in that the calcium phosphate apatite phase in bone is highly substituted with a wide range of ions.

A wide range of ions, both cations and anions, may also substitute into the structure of synthetic HA, replacing calcium (Ca), phosphate, or hydroxyl ions [2]. The substitutions alter the crystal structure to a degree, inducing some structural disorder, and so also change some of the material properties, including phase stability, solubility, and reactivity. With respect to its biological use, this can also change the material's surface characteristics (which may impact on adsorption properties, important in the interaction of the biomaterial with ions and molecules within the body), bioactivity, and biocompatibility [3-5].

Strontium is a desirable and topical ion for substitution into hydroxyapatite, showing a range of biological effects, such as improved solubility of the biomaterial [6, 7], antiresorptive activity [8], osteoclast apoptosis (osteoclasts being a main agent of bone resorption) [9] and osteoblast stimulation [9,10], thus encouraging new bone growth.

These effects potentially offer help in the treatment of osteoporosis [6, 8]. The biological activity of Sr-substituted HA is also related to effects on crystallinity [11] and expansion of its crystal lattice [7] caused by the larger size of Sr compared to Ca.

The increasing interest in Sr incorporation into biomaterials for hard tissue repair is justified by the growing evidence of the beneficial effect of this ion on bone, such as increased levels of cell proliferation, alkaline phosphatase (ALP) and collagen type I, and decreased production of interleukin-6 in rat osteoblast cultures [12, 13]. Capuccini *et al.* [14] demonstrated that human osteoblast cells (MG-63) grown on Sr-doped HA displayed normal morphology, good proliferation and increased values of the differentiation parameters, whereas the number of osteoclasts was negatively influenced by the presence of Sr [14]. The positive effect of Sr ions on bone growth was particularly evident in the case of coatings deposited from HA at relatively high Sr contents (Sr substitution for Ca at 3–7% in thin films prepared by pulsed–laser deposition), where significantly increased values of ALP activity, osteocalcin and type I collagen expression by osteoblasts, and considerably reduced values of osteoclast proliferation, were observed [14].

Table 1 summarizes the most important literature works concerning synthesis and physico-chemical characterization of Sr-substituted HA.

It shows that a great number of papers on the synthesis (with different methods) and physico-chemical characterization of Sr-HA have been reported, but with often discordant data. Literature data on Sr-substituted apatite prepared with different methods shows the formation of different products. In the case of Sr-HA prepared by a hydrothermal method a pure apatite phase is shown, independent of the molar (Ca/Sr) ratio [15-18]. On the contrary, in Sr-HA prepared by an aqueous precipitation method [5,11,19-21] or by ion exchange [6] α-TCP and β-TCP phases, respectively, are present as a function of Sr content. In the paper written by Lagergren *et al.* [22] concerning Sr-substituted HA (nominal compositions of Ca_7Sr_3HA and Ca_6Sr_4HA) prepared by a solid state method, the identification of the crystalline phases is not complete, because there are some diffraction peaks not clearly identified. Zeglinsky *et al.* [23] recently investigated Sr-substituted HA by *ab initio* methods and Rietveld analyses and reported that with high-temperature calcination, typical of solid state synthesis, the most energetically preferred substitution pattern is mixed Ca-I and Ca-II substitution, whereas for a low-temperature wet chemical synthesis, the contribution of the entropy of mixing to the stabilisation of the system is smaller but still sufficient to neutralise the endothermic nature of Sr substitution. At a temperature of 90°C the mixed arrangement is still slightly favourable.

In order to better clarify the role played by Sr addition on the physico-chemical properties of Sr-HA materials we have prepared compositions of Sr-substituted HA by a solid state method. The samples have been characterized with different techniques: *i)* X-ray powder diffraction (XRPD); *ii)* X-ray photoelectron spectroscopy (XPS); *iii)* specific surface area measurements; *iv)* Fourier transform infrared (FT-IR) adsorption spectroscopy; *v)* confocal micro-Raman spectroscopy.

After different times of reaction in cell culture medium, the solutions were analyzed by inductively coupled plasma – atomic emission spectroscopy (ICP-AES) in order to evaluate the ion release in solution from the studied materials, while the reacted powders were characterized by *i)* FT-IR spectroscopy, *ii)* confocal micro-Raman spectroscopy, and *iii)* environmental scanning electron microscopy - energy dispersive spectroscopy (ESEM-EDS).

In the literature (see references reported in **Table 1**), only a few of the experimental techniques listed above were used to characterize the Sr-substituted samples.

The present work also studied the effects produced by Sr-substituted HA on human osteoblast-like cells (MG-63). Cytotoxicity, measured as release of lactate dehydrogenase (LDH), cell proliferation (tritiated thymidine method) and cell differentiation (ALP activity, as an early expression of a more differentiated state) were evaluated after incubation of different amounts of HA and Sr-HA samples for different times. To assess the effects of Sr ions *per se*, the same experiments were also carried

out after incubation of cells in medium containing amounts of $SrCl_2$ that mimic the amount of Sr ions released from the Sr-HA samples.

2. Experimental section: Materials and Methods

2.1 Materials

Pure and substituted HA specimens were prepared by a solid state method.

The synthesis was carried out on a 10g scale. Desired compositions and molar concentrations of reactants used are given in **Table 2**.

Calcium hydrogen phosphate ($CaHPO_4$, Merck, 98.0–100.5%) and calcium carbonate ($CaCO_3$, Sigma-Aldrich, 99+%) were thoroughly mixed and homogenized with a pestle and mortar. Sr-substituted HA samples were prepared by replacing a portion of $CaCO_3$ with an equivalent molar amount of strontium carbonate ($SrCO_3$, Aldrich, ≥99.9% metals basis).

The powders were then pressed into pellets (~1 g of reagent mixture, using a 13 mm die) and reacted in a high temperature furnace (Carbolite, UK). The furnace program involved heating the reaction mixtures from 200 to 1100˚C at 10˚C/min, holding at 1100˚C for 16 hours, followed by cooling the products from 1100 to 200˚C at 10˚C/min and then air-cooling to room temperature.

2.2 Characterization of synthesized samples

2.2.1 X-ray Powder Diffraction (XRPD)

XRPD analysis was performed on powder samples using a Bragg-Brentano diffractometer (PANalytical X'Pert Pro with Ni-filtered Cu K_α radiation, 10-60° 2θ range, and a counting time of 50s for each 0.03° 2θ step). Diffraction patterns were compared to ICDD database PDF patterns for HA (JCPDS n° 09-432, ICDD, Newton Square, Pennsylvania, U.S.A), Sr-substituted HA of stoichiometry $Ca_8Sr_2(PO_4)_6(OH)_2$ (JCPDS n° 34-0483), and Sr-substituted HA of stoichiometry $Ca_6Sr_4(PO_4)_6(OH)_2$ (JCPDS n° 34-0480).

Crystallite size, *d*, was determined by Debye–Scherrer formula [25] as reported in eq. (1):

$$\boldsymbol{d} = \frac{0.9\lambda}{\boldsymbol{w}\cos\theta} \quad (1)$$

where *w* stands for the full width at half maximum value (FWHMs), λ is the diffraction wavelength (1.5405 Å), and θ is diffraction angle at the (002) *hkl* reflection.

The crystallinity degree, corresponding to the fraction of crystalline phase (Xc) in powders, was evaluated by the following equation (2) [26]:

$$X_c \approx 1 - \frac{V_{112/300}}{I_{300}} \quad (2)$$

where I_{300} is the intensity of (300) *hkl* reflection and $V_{112/300}$ is the intensity of the hollow between (112) *hkl* and (300) *hkl* reflections.

Rietveld refinement was performed with GSAS [27] and EXPGUI [28].

Initial atomic coordinates and unit cell dimensions were taken from previously published data [29].

Parameters varied in the refinement were atomic coordinates (x, y and z), unit cell parameters (a and c), displacement parameters (Uiso), peak intensity scaling and peak profile parameters related to particle size.

2.2.2 X-ray photoelectron spectroscopy

XPS spectra were recorded using an M-probe apparatus (Surface Science Instrument) with a monochromatic Al K_R source (1486 eV). A spot size of 400 x 1.000 μm, a pass energy of 150 eV and a resolution of 1.39 eV were used. Measurements for each sample were taken over three spots and averaged. The accuracy of the reported quantitative data (atomic percentage) can be estimated to be ± 1 % [30]. By this technique, the surface presence of elements that composed the bulk materials (Ca, P, O, Sr) could be investigated and quantified.

2.2.3 Environmental scanning electron microscopy - Energy dispersive spectroscopy (ESEM-EDS).

The actual composition of synthesized materials was determined by means of ESEM (FEI Quanta 200, Fei Company, The Netherlands), equipped with an EDS instrument (INCA 350, Oxford Instruments, UK). For each composition, two different samples were analyzed, and the EDS analysis was performed over 4 different sample areas.

2.2.4 Specific surface area (SSA) measurements

SSA was evaluated using a Micromeritics ASAP 2020 porosimeter, by adsorption of an inert gas (Kr) at 77 K. For the materials prepared by solid state synthesis, which possess very low SSA, Kr was used as the adsorptive gas rather than N_2 because Kr can be conveniently used to measure small adsorbed amounts (and thus small SSAs) because it has a low saturation vapour pressure and, therefore, the “dead space” correction for unadsorbed gas is also small and allows reasonable precision in the adsorption measurement [31]. Before measurements, all samples were inserted into the cell in the powder form and were activated *in vacuo* (residual pressure < 10^{-3} Torr) at room temperature for 12 h in order to remove physisorbed atmospheric contaminants. Crushing the samples during preparation did not influence the SSA values obtained.

For SSA determination, data were analyzed with the BET model [32]. The accuracy of the conventional BET method/model for SSA determination is known to be relatively low (±5% divergence from the actual area), even if the instrumental accuracy and reproducibility of data obtained with modern automatic gas-volumetric instrumentation are quite high [31].

2.2.5 Fourier transform infrared adsorption spectroscopy.

IR absorption spectra were obtained using a FT-IR spectrometer (Bruker IFS 28, equipped with both MCT and DTGS detectors) in the 4000-400 cm^{-1} spectral range. The powdered materials were diluted with spectroscopic grade KBr powder (approximately 1 mg of sample to 50 mg of KBr) and pressed into pellets, to allow even the most intense bulk absorption bands to be observed. The pellets, protected by a gold-frame envelope, were placed in a quartz cell equipped with KBr windows, which are transparent to IR radiation above ~400 cm^{-1}. Transmission spectra were recorded using the DTGS detector, so that the low-frequency region might be inspected. For each measurement, 128 scans at resolution 4 cm^{-1} were performed.

2.2.6 Confocal micro-Raman spectroscopy.

Micro-Raman spectra were acquired using an integrated confocal Raman system that includes a Horiba Jobin-Yvon HR800 microspectrometer, an Olympus BX41 microscope, and a CCD air-cooled detector operating at -70˚C. A polarized solid-state Nd laser, operating at 532.11 nm and 80 mW, was used as the excitation source. Correct calibration of the instruments was verified by measurement of the Stokes and anti-Stokes bands and checking the position of the Si band at 520.7 cm^{-1}. To optimize the signal-to-noise ratio, spectra were acquired using an integration time of about 100 s for each spectral region. Spectra were collected over the range 1300-400 cm^{-1}.

2.3 Sample reactivity in cell culture medium

Minimum Essential Medium Eagle with Earl's salts (MEM), the cell culture medium (Sigma–Aldrich) used for MG-63 culture, contains inorganic ions, like those present in simulated body fluids (SBF) solutions, and mimics the inorganic ion composition of human plasma. The main difference between SBF and MEM is the HCO_3^- concentration, which is 4.2 and 44.0 mM, respectively [34]; MEM also contains amino acids, vitamins, glucose, L-glutamine and Na pyruvate. The use of this complex solution, mimicking the cellular environment, allows assessment of the reactivity of the test materials usually tested with SBF solutions while also simultaneously observing any other reactivity effects that may occur during cell culture. The pH was set to 7.4.

2.3.1 Soaking in cell culture medium

To evaluate the changes in the samples after immersion in cell culture medium, they were soaked in the amounts of 200 and 500 μg/ml in MEM buffered solution. Samples were immersed in a sterile polyethylene test bottle containing MEM solution and kept at 37°C under continuous stirring for 1, 7 and 14 days.

2.3.2 Inductively coupled plasma – atomic emission spectroscopy (ICP-AES) measurements.

Solutions derived from each of the above soaking treatments were filtered with a 0.45 μm Advantec MFS membrane filter. The clear filtrate obtained was analyzed for Ca, Sr and phosphorus (P) by ICP-AES with a Varian Liberty Series II instrument working at the following wavelengths (relative to the emission of each species): Ca, 422.673 nm; Sr, 407.771 nm; PO_4, 214.914 and 213.617 nm. The standard used for the calibration curves was a Certipur (Merck) ICP multi-element standard of concentration 1000 mg/L in diluted HNO_3. Ca and PO_4 concentrations at day 0 found in MEM were 72 and 85 ppm respectively [34]. These values have been subtracted from that found at the different soaking times.

2.3.3 Scanning electron microscopy

After filtration, SEM was used to investigate any effect of soaking the powder samples in MEM solution on their surface morphology. The images were obtained with a ZEISS ECO 50 XVP microscope equipped with a LaB6 source, with acquisition of images at 15 kV.

2.4 Cellular tests

2.4.1 Cells and reagents

MG-63 human osteoblast cells (provided by Istituto Zooprofilattico Sperimentale "B. Ubertini", Brescia, Italy) were cultured to near-confluence in 35-150 mm diameter Petri dishes with MEM supplemented with 10 % foetal bovine serum (FBS), penicillin, streptomycin and L-glutamine in a humidified atmosphere containing 5% CO_2 at 37°C. Before the assays, the confluent cells were incubated for 1, 7 and 14 days in the absence or presence of the HA/SrHA samples and other reagents, as described in the following paragraphs. In our experiments, all powders were suspended in MEM at 1 mg/ml, sonicated (Labsonic sonicator, 100 w, 10 s) before each incubation, and then incubated with the cells, by diluting the suspension in the dishes with supplemented MEM (i.e. MEM containing FBS and antibodies) to different concentrations (indicated below). This procedure does not modify the physicochemical characteristics of the samples, but ensures their better suspension in the culture medium. The cells were also incubated for 1, 7 and 14 days in the absence or presence of different concentrations of $SrCl_2$, corresponding to the concentrations of Sr^{2+} released by the powders in MEM and determined by ICP-AES.

The protein contents of cell monolayers and cell lysates were assessed with a BCA kit (Pierce, Rockford, IL). Plasticware was from Falcon (Becton Dickinson, Franklin Lakes, NJ). Unless otherwise specified, other reagents were purchased from Sigma Aldrich (Milan, Italy).

2.4.2 Lactate dehydrogenase (LDH) leakage

To check the cytotoxic effect of the different experimental conditions described in the Results section, LDH activity was measured from aliquots of culture supernatant and in the cell lysate at the end of the 1, 7 and 14 day incubation times in the absence or presence of apatite samples and other reagents ($SrCl_2$), as described previously [24]. Both intracellular and extracellular enzyme activities, measured spectrophotometrically as absorbance variation at 340 nm (37°C), were expressed as μmol of reduced nicotinamide adenine dinucleotide (NADH) oxidized/min/mg cell protein, then extracellular LDH activity was calculated as a percentage of the total (intracellular + extracellular) LDH activity.

2.4.3 H^3- thymidine proliferation assay

After 7 days of incubation with apatite samples or $SrCl_2$ (used at the highest Sr concentration released from apatite samples at 7 days at each of the two different concentrations) the H^3-thymidine proliferation assay was performed by the modified method described elsewhere [35].

This test allows determination of the number of cells that are growing in the absence or presence of HA/Sr-HA samples or $SrCl_2$. The principle of this assay was: cells were seeded in the wells of a 96 well plate, incubated for 1 day at 37°C, then H^3-thymidine (1 µCi/well H^3-thymidine corresponding to 5 µCi/ml) was added to the wells and incubated for 6 days at 37°C, without removing the different samples from the culture medium. During each cell division the cells will incorporate H^3-thymidine into DNA. The more cell divisions (or the higher the proliferation rate) the more radioactivity will be incorporated into DNA. After incubation the cells were harvested by adding 0.3 M NaOH and, to the detached cells, 5 ml of scintillation fluid; the radioactivity was measured in a β-counter. The % increase of cell proliferation was thus calculated.

2.4.4 Alkaline phosphatase (ALP) activity

After 7 days of incubation with the HA/Sr-HA samples or $SrCl_2$ (used at the highest Sr concentrations released from apatite samples at 7 days at both different concentrations) ALP activity was assessed in cell culture medium using the QuantiChrom™ alkaline phosphatase assay kit (Gentaur – DBA Italia, Milan, Italy). Briefly, the method utilizes p-nitrophenyl phosphate (pNPP) that is converted by ALP to an equal amount of colored *p*-nitrophenol (*p*NP), a soluble yellow end-product measurable at 405 nm. The ALP activity was expressed as µmol of *p*NP formed in 1 min/ mg cell protein.

2.4.5 Statistical analysis

All data in the text, tables and figures are provided as means ± SE. The results were analyzed by one-way analysis of variance and Tukey's test. $P < 0.05$ was considered significant.

3. Results and Discussion

3.1 Characterization of synthesized samples

3.1.1 X-Ray Powder Diffraction.

The collected diffraction patterns of reacted samples are reported in **Figure 1.** Peak positions and relative intensities of the three traces correspond very well to those of the ICDD PDF patterns for HA (trace 3), Sr-substituted HA of stoichiometry $Ca_8Sr_2(PO_4)_6(OH)_2$ (trace 2), and Sr-substituted HA of stoichiometry $Ca_6Sr_4(PO_4)_6(OH)_2$ (trace 1). Patterns of HA and x=2 Sr-HA showed only diffraction peaks that matched the corresponding apatite phases, with no impurity phases. For the pattern of $Ca_6Sr_4(PO_4)_6(OH)_2$, there was a small amount of β-TCP observed as a peak at approximately 30.5° 2θ, but no unidentifiable diffraction peaks were observed, in disagreement with the data previously reported [22]. These results indicate that only Sr-substituted HA was formed by this synthesis route for x=2 and Sr-HA with a small amount of β-TCP for x=4.

In **Table 3,** some parameters obtained from the XRD patterns are shown.

The partial substitution of Sr for Ca, in order to obtain a solid solution, as already reported by O'Donnell [36], is clearly evidenced by the shift of the diffraction peaks to lower 2θ values with Sr addition, indicating a gradual increase in d-spacing (see the inset in **Figure 1**, and the d-spacings reported in **Table 3**).

The effect of strontium substitution is also evidenced by the increase of the cell parameters (**Table 3**) obtained from Rietveld refinement. This is to be expected, as Sr is a slightly larger ion than Ca (118 and 100 pm, respectively, for octahedral coordination) [37]. Peak intensity decreased with Sr addition: this result disagrees with that of another report [36], where the addition of Sr caused an increase of the peak intensities. This disagreement and apparent contradiction could be possibly due to a different synthesis method route used in this paper respect to those used from O'Donnell and co-workers (by a wet chemical route and lower temperature).

The crystallite size, *d,* as reported in **Table 3**, decreased with Sr addition, and this is consistent with the results reported [5,36], which observed that the substitution of Sr (50% and 15%, respectively) caused an appreciable decrease in crystallite size.

The addition of Sr gives also rise to a decrease of the crystallinity degree, *Xc*, and this trend is certainly consistent with the overall peak intensity decrease reported and discussed below (see also Raman spectra).

3.1.2 Specific surface area measurements.

SSA of the HA/Sr-HA materials (reported in **Table 4**) is very low (in the 0.6 – 1.2 m^2/g range) and no pores are present, as a result of the long reaction period at high temperature which allowed

significant particle sintering and crystal growth. For SSA determination the data was analyzed with the standard BET model [32] and, as is well known, the accuracy of the universally adopted BET method is ± 5%, whereas the instrumental accuracy with modern automatic gas-volumetric instrumentation is quite high (± 0.1 %). By the inspection of SSA data reported in **Table 4,** taking into account the standard deviations, it is possible to note that the introduction of increasing amounts of Sr in the HA composition caused a decrease in SSA. As also reported in the work by Kolmas *et al.*[38], the BET results could be affected by compact crystal aggregation. In our case the Sr^{2+} incorporation probably had a slight influence on crystal dimensions and/or aggregation.

3.1.3 X-ray photoelectron spectroscopy.

Data from elemental analysis measurements by XPS of the surfaces of HA/Sr-HA materials are shown in **Table 5, Part A;** data are reported as atomic %.

All materials contained abundant carbon (C). This is likely to be present as aliphatic hydrocarbonaceous residues present in the environment, as often found with oxide materials and already reported in our previous XPS analysis [30,39]. In fact, in the case of bioactive glasses, the amount of C has been found to be present at the surface of these materials as a consequence of the formation of carbonate like species and/or surface contaminants. HA materials were synthesized by a method involving $CaCO_3$ as a reactant, but the high temperature involved in the synthesis method should have caused all the CO_3^{2-} to be driven off as CO_2. However (part of) the high C% could be also due to (surface) carbonatation (CO_3^{2-}) of the material, deriving from carbon dioxide (CO_2) present in the air. It is possible that some CO_3^{2-} was taken up onto these materials during cooling in air after synthesis, and in the same way the materials may have absorbed aliphatic hydrocarbons. Both hydrocarbons and CO_2 may have been picked up during storage and the measurement procedures. In either case the contaminants are unlikely to be structural and are most probably adsorbed at the surface of the material particles.

If we consider only the atomic % of the elements other than C (O, Ca, Sr and P), we can observe that the amount of surface metal ions (Ca+Sr) increases with increasing Sr content, but is always lower than the theoretical value obtained by the nominal composition [(Ca+Sr) = 23.8]. At the same time, as a function of Sr addition there is also an increase of the P amount, although the amount of P is also always lower than that of the nominal sample composition.

Table 6 reports some molar ratios, as calculated from the data from both XPS and EDS elemental analysis, in comparison with the corresponding theoretical ones. The sample of composition $Ca_6Sr_4(PO_4)_6(OH)_2$ is enriched in surface Sr [the observed Sr/Ca ratio (0.79) (see **Table 6**) is larger than expected (0.67)] but, at the same time, the overall surface concentration of metal ions (as

represented by M/P and Ca/P ratios) is depleted. The relative Sr enrichment may be related to the localization of a Sr-apatite phase at the surface, and the overall metal depletion is likely to be linked to the presence at the surface of a CaP phase with a Ca/P ratio lower than the ratio for stoichiometric HA.

3.1.4 ESEM-EDS.

The compositions determined by EDS analysis, reported in **Table 5**, correspond very well to the nominal ones. Still, the samples seem to present a rather non-homogeneous distribution of the elements, as evidenced by the high standard error values (± SE). This is particularly true in the case of Ca in the samples $Ca_{10}(PO_4)_6(OH)_2$ and $Ca_6Sr_4(PO_4)_6(OH)_2$. The molar ratios calculated from EDS analysis, reported in **Table 6**, are more similar to those of the nominal composition compared to the value obtained with data from XPS analysis. These data provide evidence that the surface composition (XPS data) of the materials is significantly different to that of the bulk (EDS data).

3.1.5 FT-IR spectroscopy.

FT-IR spectra of HA and Sr-substituted HA can be viewed in **Figure 2**. The bands at ~430 cm^{-1} can be assigned to the ν_2 mode of (PO_4^{3-}); the bands at ~570, ~610 and 630 cm^{-1} to the ν_4 mode of (PO_4^{3-}); and the band at ~960 cm^{-1} to the ν_1 mode of (PO_4^{3-}). The bands at ~1050 (broad and complex) and ~1090 cm^{-1} (sharp shoulder) were due to the ν_3 mode of (PO_4^{3-}) and/or the ν_1 mode of (CO_3^{2-}).

It is quite evident that there are no significant spectral differences between Sr-HA systems and the reference HA system. In particular, all of the samples show only the bands typical of a pure HA composition, with only trace amounts of (CO_3^{2-}) impurities; for example, no vibration at ~870-880 cm^{-1} for the ν_2 mode of (CO_3^{2-}) was observed for any of the samples.

3.1.6 Raman spectroscopy.

The Raman spectra collected for all materials are shown in **Figure 3**.

The bands at ~420, ~580 and ~960 cm^{-1} could be assigned to the ν_2, ν_4, and ν_1 (PO_4^{3-}) lattice modes, respectively. The band at ~1050 cm^{-1} was consistent with the ν_3 lattice modes of (PO_4^{3-}) and ν_1 lattice modes of (HPO_4^{2-}), as well as with the ν_3 mode of (CO_3^{2-}). Finally, the weak band at ~1080 cm^{-1} was ascribable to the A-type ν_1 mode of (CO_3^{2-}) [40].

These bands, observed for all of the examined samples, were consistent with those of HA.

The main analytical Raman band of (PO_4^{3-}), due to the totally symmetric ν_1 mode, was observed to shift from 962 cm^{-1} in stoichiometric HA to 959 cm^{-1} in $Ca_8Sr_2(PO_4)_6(OH)_2$ and to 956 cm^{-1} in

$Ca_6Sr_4(PO_4)_6(OH)_2$ (see **Figure 3B**). This shift, consistent with the larger mass of Sr with respect to Ca, is similar in magnitude to that observed by O'Donnell *et al*. [36] [from 963 cm^{-1} in HA to 956 cm^{-1} in $Ca_{2.5}Sr_{2.5}(PO_4)_3(OH)$].

Increasing the amount of Sr, the v_1 Raman band of (PO_4^{3-}) was also observed to become weaker and broader in comparison with the same band in stoichiometric HA. The broadening is consistent with a decrease of crystallinity, already monitored by XRD, brought about by the introduction of Sr.

3.2 Bioactivity in MEM

3.2.1 ICP data.

ICP data concerning Sr, Ca and P release from HA/Sr-HA samples after different soaking times in cell culture medium at the concentrations of 200 and 500 μg/ml (corresponding to the 50 and 125 $\mu g/cm^2$ concentrations, respectively, used in cellular tests) are reported in **Table 7** and **Figure 4**. Inspection of ICP data shows that the ion release (Ca, Sr and P) was quite similar for all samples; but the day 1 values of Ca and P for the Sr-HA samples are low compared to the HA sample at day 1. The level of ion release was affected by the concentrations used for the soaking tests. Ni et *al.* [41] observed increasing solubility of HA ceramic after Sr incorporation, in their work having added 0.2 g/ml of Sr-substituted HA powder to 10% FBS L-DMEM culture medium and incubated at 37 °C for 24 h.

At the highest concentration used (500 μg/ml), between 7 and 14 days of soaking time for all samples in the present study there was a decrease of Ca, Sr and P concentrations in solution; these data could be an indicator of calcium phosphate or calcium/strontium phosphate precipitation on the material's surface during soaking/reaction in MEM.

3.2.2. Scanning electron microscopy (SEM).

Figure 5 reports SEM images of all the samples studied as prepared and after 2 weeks of reaction in MEM solution. Both of the materials substituted with Sr showed changes in particle size or morphology during the first two weeks of soaking: they formed very large aggregates (hundreds of μm in size) of particles (sub-μm in size). Ion release from the surface of powder particles during soaking results in surface charge or instability and the reprecipitation of these particles on the surface. On the contrary, the morphology of the pure HA does not change after 2 weeks of soaking/reaction in MEM.

3.3 Cellular tests

To test for any potential cytotoxic effects of the materials at different concentrations and incubation times, HA, Sr-substituted HA samples and $SrCl_2$ were incubated with human MG-63 osteoblast cells and LDH release was evaluated (see **Figure 6**). The release of LDH in extracellular medium is a sensitive index of cytotoxicity. After 1 day of incubation no significant changes in the LDH release were observed. On the contrary, in the case of the two Sr-HA samples, after 7 and 14 days incubation time there was a significant decrease in the LDH release. Since LDH data are reported as percentage of extracellular LDH vs the total LDH (extracellular + intracellular LDH), the decrease of released LDH observed after 7 and 14 days with Sr-HA samples was mainly attributable to an increase of intracellular LDH; this result indicates an increase of cell proliferation in the presence of Sr-HA compared to the HA sample, as confirmed by the subsequent experiments (see below). From these data we can state that addition of Sr to HA does not cause any cytotoxic effect on MG-63 cells.

To study the effect of Sr alone on MG-63 cells, the LDH production was measured after 1, 7 and 14 days of cell incubation in MEM supplemented with amounts of $SrCl_2$ corresponding to the amounts of Sr released from the Sr-HA (200 and 500 μg/ml) after 1, 7 and 14 days incubation in MEM alone (see **Table 7**). $SrCl_2$ did not cause appreciable changes in the LDH release at the times and concentrations investigated.

To better evaluate the cell proliferation we also performed the H^3-thymidine assay (see **Figure 7).** This was performed after 7 days of incubation only because after 7 days soaking in MEM solution at 200 and 500 μg/ml we found the highest concentration of Sr ions. For the samples incubated at the concentration of 500 μg/ml of powder in MEM, after 7 days we observed a re-precipitation of a Ca/Sr-P phase from the MEM solution onto the materials' surfaces. No differences emerged between cells cultured on polystyrene alone (control) and cells cultured in MEM supplemented with $SrCl_2$. Conversely, the presence of Sr-HA materials at 50 and 125 $\mu g/cm^2$ of cell monolayer significantly increased the cell proliferation after 7 days compared to the control and to the data obtained with the HA sample. The results of ALP activity, expressed as mg cell protein and measured in the same experimental conditions as the H^3-thymidine assay, are reported in **Figure 8**. There was no statistical difference in ALP activity after 7 days incubation with the HA and Sr-HA materials at both concentrations used and with the concentrations of $SrCl_2$ compared to the control. However, a different data profile was observed to the data profile in **Figure 7** showing the increased cell proliferation in presence of two Sr-HA materials. Our data confirm the literature data [12,42-44] that suggested that Sr contained in biomaterials has the potential to increase osteoblast proliferation [43].

Although Sr incorporation in various materials enhances the cell proliferation, the optimal Sr concentration remains controversial. Park *et al.* [45] found that Sr ions released at 103-135 ppb enhanced the differentiation of osteoblasts. Ni *et al.* [41] evidenced a positive effect using Sr concentrations of 5 ppm [41] and in other works [46-48] concentrations of 17.5 ppm or above of Sr are required to enhance osteoblast proliferation. On the other hand Braux *et al.* [43] demonstrated that after 7 days of incubation with $SrCl_2$ in the range 10^{-6}–10^{-3} M the cell proliferation was enhanced.

Our data suggest that Sr alone at concentrations between 1.21 and 3.24 ppm does not influence the proliferation of MG-63 cells. Thus, the other ions released from a Sr-substituted material might co-act with Sr ions [49, 50]. In addition to producing elevated levels of Sr ions in the MEM, soaking the Sr-HA samples resulted in significantly lower concentrations of both calcium and phosphate ions in the MEM after 7 days of soaking, at both Sr substitution levels and at both powder/MEM ratios, compared to the HA sample (**Table 7**). Further investigation is needed to identify if the role of Sr ions on both osteoblast and osteoclast cells is mediated by concomitant concentrations of calcium and phosphate ions in the culture medium.

Conclusions

Compositions of Sr-substituted HA prepared by a solid state method have been studied in order to better clarify the role played by the addition/substitution of Sr on the physico-chemical properties of the apatitic materials. For the first time, the samples of interest have been characterized with a large number of different and complementary techniques.

XRD characterization indicates that the addition of Sr influences the structure of HA, with evidence of a decrease in the crystallinity degree; this trend is consistent with the overall peak intensity decrease reported and also with Raman results.

From FTIR and Raman data no changes in the spectra were observed in soaked samples compared to un-soaked samples (data not shown for sake of brevity), whereas from SEM images it is possible to identify that the materials substituted with Sr (but not the unsubstituted HA samples) showed changes in particle size or morphology during the first two weeks of soaking: they formed very large aggregates (hundreds of μm in size) of particles.

Concerning *in vitro* cellular tests, we confirm that the presence of partial substitution of Sr in HA has a positive effect on MG-63 cells, but these effects are probably due to the co-action of other ions (Ca and P) along with Sr to favour only the cell proliferation and not to enhance cell differentiation, since Sr ions (from supplementation of the medium with $SrCl_2$) alone did not influence the proliferation of MG-63 cells. For this reason further detailed studies are needed to understand the role carried out by other ions dissolved from the biomaterials.

Thus our research findings confirm that metal ion dopants can allow controlled design of the properties of synthetic bone graft materials.

Figure Captions.

Figure 1. Section A: XRD patterns of the 10 - 60° 2θ range of materials prepared by solid state synthesis. 1: $Ca_6Sr_4(PO_4)_6(OH)_2$; 2: $Ca_8Sr_2(PO_4)_6(OH)_2$; 3: $Ca_{10}(PO_4)_6(OH)_2$. Intensity is reported in arbitrary units. Traces have been y-axis shifted for display purposes. **Section B:** details in the 30.5 - 34.5° 2θ range.

Figure 2. FT-IR spectra (KBr pellet method; 1400-400 cm^{-1} spectral range) of the following samples: 1. $Ca_{10}(PO_4)_6(OH)_2$, 2: $Ca_8Sr_2(PO_4)_6(OH)_2$, 3: $Ca_6Sr_4(PO_4)_6(OH)_2$.

Figure 3. Micro-Raman spectra in the 1300-400 cm^{-1} range (Section A) of the following synthesized samples: 1. $Ca_{10}(PO_4)_6(OH)_2$, 2: $Ca_8Sr_2(PO_4)_6(OH)_2$, 3: $Ca_6Sr_4(PO_4)_6(OH)_2$. Section B: blown-up segment in the 1000-900 cm^{-1} range [the totally-symmetric ν_1 mode of (PO_4^{3-})].

Figure 4. ICP data of all the studied samples after different soaking times in MEM solution are reported. Ions concentrations are reported as ppm. **Section A:** Released data at sample concentration of 200 μg/ml; **Section B:** Released data at sample concentration of 500 μg/ml. Square: Ca ions; circle: P ions; up-triangle: Sr ions. Solid symbols: $Ca_{10}(PO_4)_6(OH)_2$; open symbols: $Ca_8Sr_2(PO_4)_6(OH)_2$ and x center symbols: $Ca_6Sr_2(PO_4)_6(OH)_2$.

Figure 5. SEM images of all samples as-synthesized and after soaking in MEM for two weeks.

Figure 6. Effect of HA/Sr-HA powders and/or $SrCl_2$ on LDH release in the supernatant of MG-63 cells. Cells were incubated in absence (CTRL) or presence of HA/Sr-HA powders at two different concentrations (200 and 500 μg/ml, corresponding to 50 and 125 $\mu g/cm^2$ of cell monolayer) and/or $SrCl_2$ (corresponding in the same order to the amounts of Sr released from the indicated Sr-HAs, as shown in Table 7) after 1, 7 and 14 days incubation time. The numbers reported over each column concerning incubation with $SrCl_2$ alone are ppm of Sr released in each incubation condition (see Table 7 for further details). Data are presented as mean ± SE (n = 3). Significance vs. the corresponding control: * $p < 0.0001$.

Figure 7. Evaluation of cell proliferation reported as % of cell proliferation vs. control, using the H^3-thymidine assay. MG-63 cells were incubated without (CTRL) or with the HA/Sr-HA samples at 200 and 500 μg/ml (corresponding to 50 and 125 $\mu g/cm^2$ of cell monolayer) and with $SrCl_2$ (corresponding to the amounts of Sr released from these Sr-HAs) for 7 days (i.e. the time period already showing the greatest release of Sr ions). The numbers reported over each column concerning incubation with $SrCl_2$ alone are ppm of Sr released in each incubation condition (see

Table 7 for further details). Data are presented as mean ± SE (n = 3). Significance vs. control: * $p < 0.0001$.

Figure 8. Alkaline phosphatase (ALP) activity of MG-63 cells after 7 days culture (*i.e.* the time period already showing the greatest release of Sr ions) without (CTRL) or with HA/Sr-HA samples at 200 and 500 μg/ml, corresponding to 50 and 125 μg/cm^2 of cell monolayer, and $SrCl_2$ (corresponding to the amounts of Sr released from these Sr-HAs). The numbers reported over each column concerning incubation with $SrCl_2$ alone are ppm of Sr released in each incubation condition (see **Table 7** for further details). Data are presented as mean ± SE (n = 3). Significance vs. control: * $p < 0.0001$.

Figures.

Figure 1.

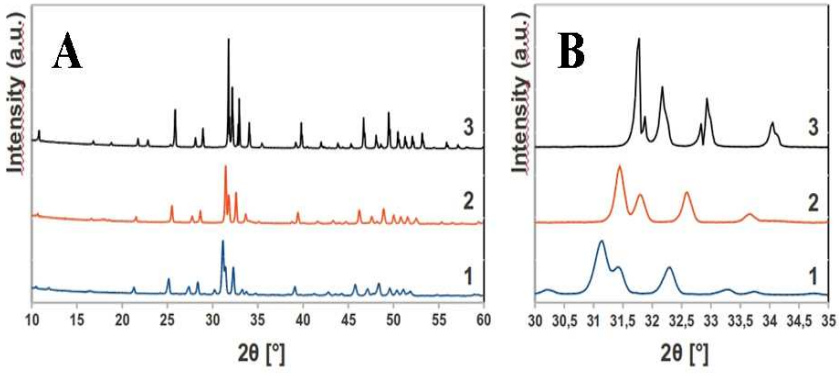

Figure 2.

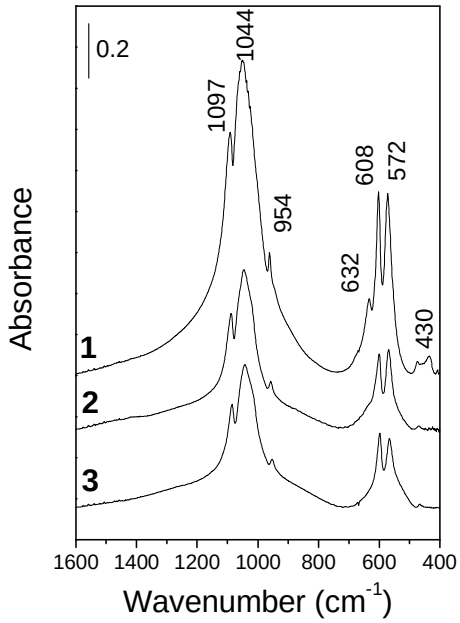
0.2
1044
1097
954
608
572
632
430
1
2
3
Absorbance
1600 1400 1200 1000 800 600 400
Wavenumber (cm-1)

Figure 3.

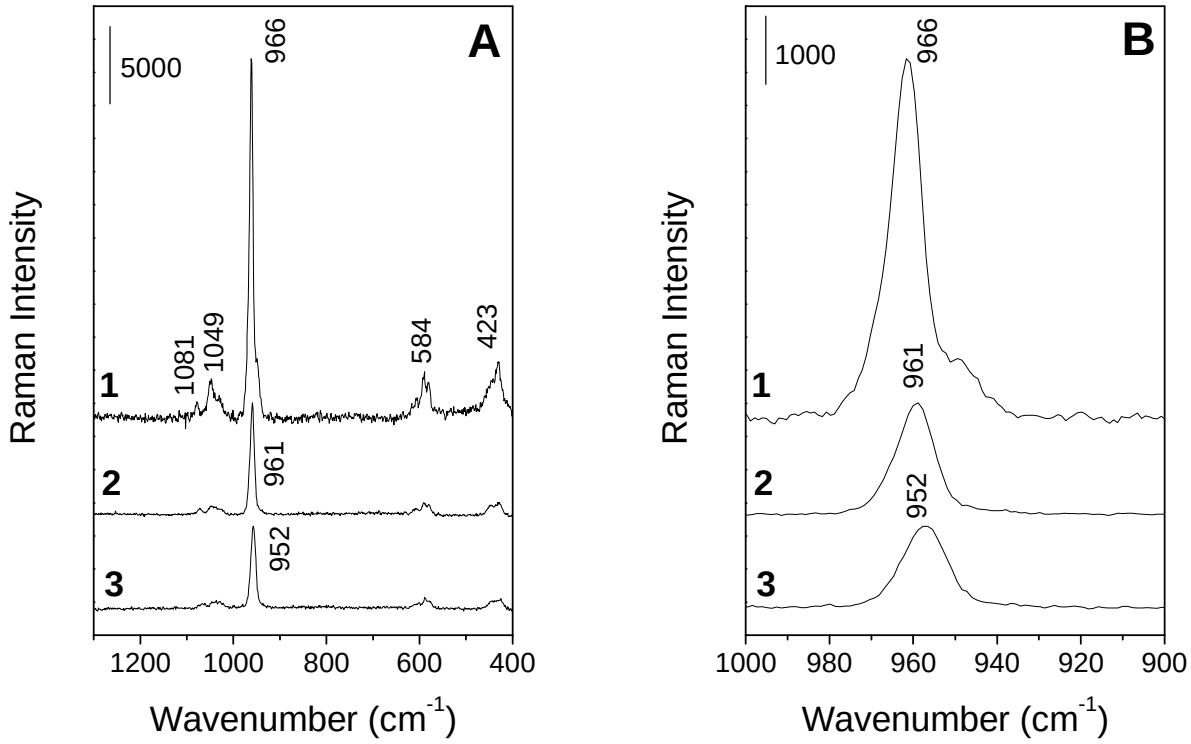
A
5000
966
1081
1049
584
423
1
961
2
952
3
Raman Intensity
1200
1000
800
600
400
Wavenumber (cm-1)
B
1000
966
961
952
1
2
3
Raman Intensity
1000
980
960
940
920
900
Wavenumber (cm-1)

Figure 4.

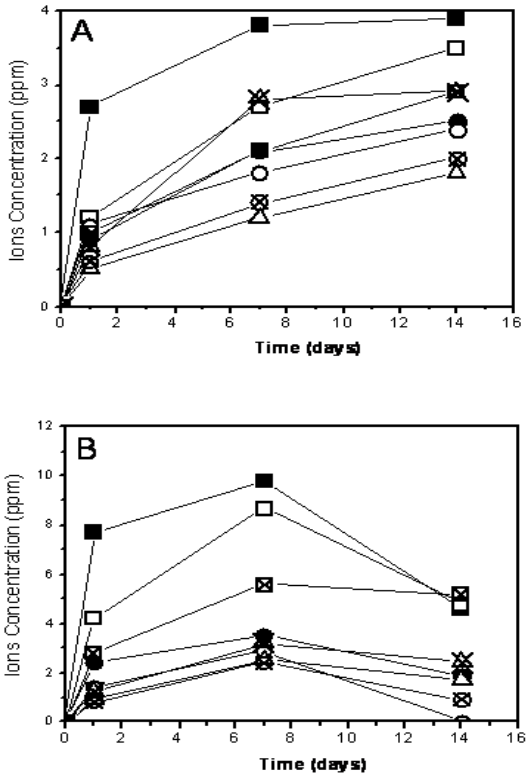
A
Ions Concentration (ppm)
Time (days)
B
Ions Concentration (ppm)
Time (days)

Figure 5.

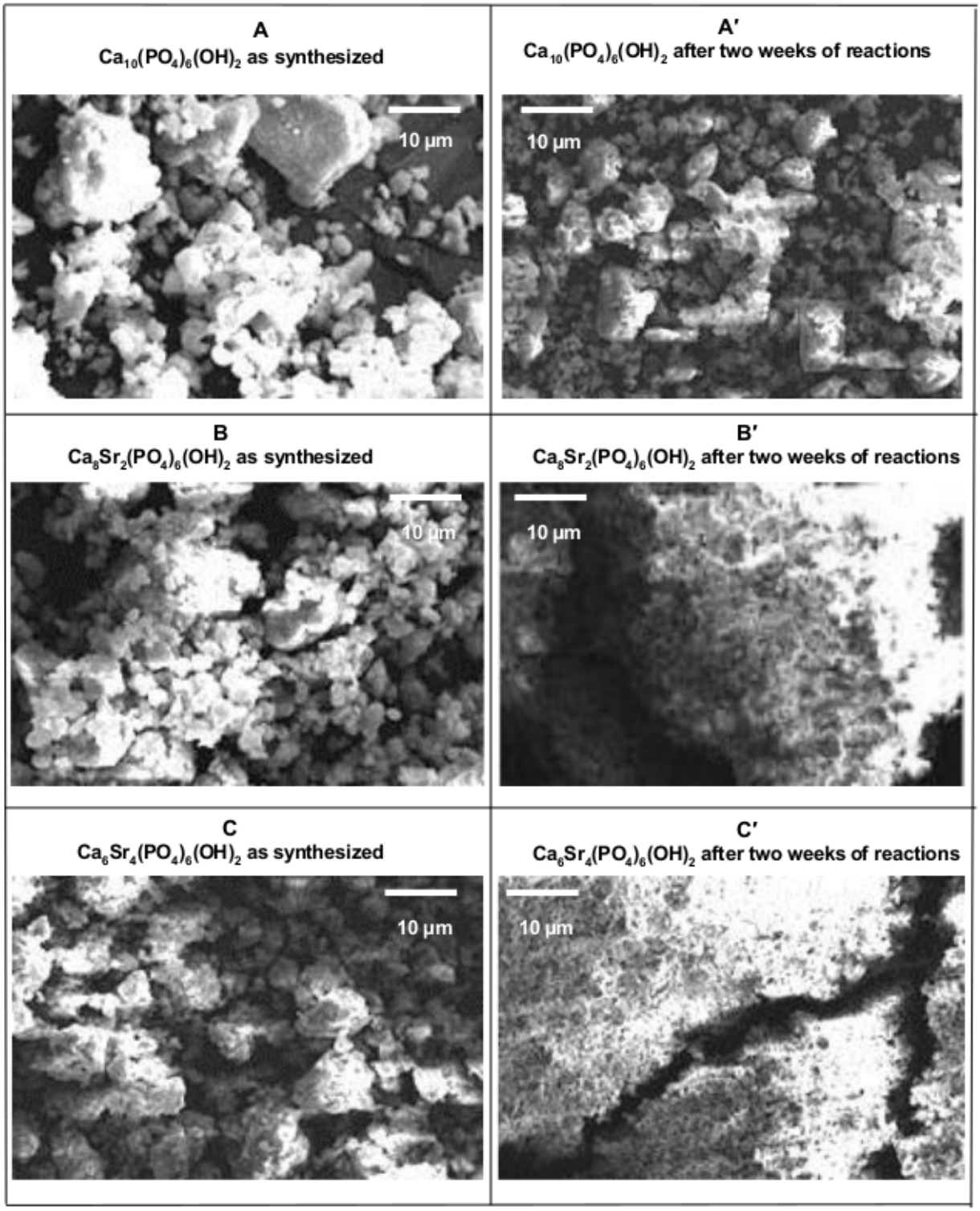
A
$Ca_{10}(PO_4)_6(OH)_2$ as synthesized
10 µm
A′
$Ca_{10}(PO_4)_6(OH)_2$ after two weeks of reactions
10 µm
B
$Ca_8Sr_2(PO_4)_6(OH)_2$ as synthesized
10 µm
B′
$Ca_8Sr_2(PO_4)_6(OH)_2$ after two weeks of reactions
10 µm
C
$Ca_6Sr_4(PO_4)_6(OH)_2$ as synthesized
10 µm
C′
$Ca_6Sr_4(PO_4)_6(OH)_2$ after two weeks of reactions
10 µm

Figure 6.

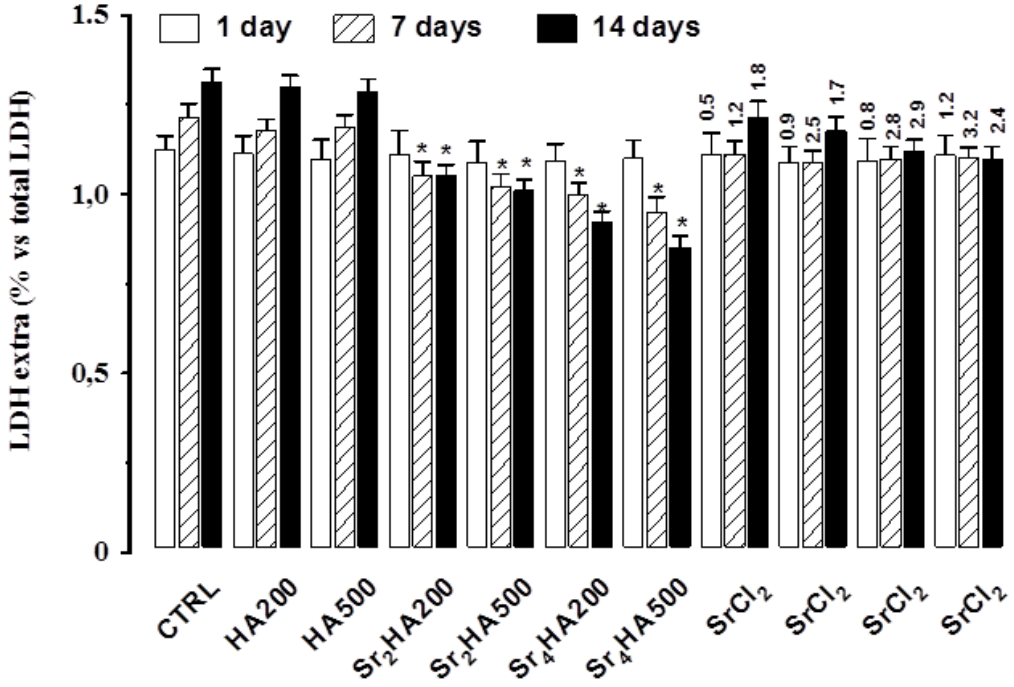
1.5
1,0
0,5
0
LDH extra (% vs total LDH)
1 day
7 days
14 days
0.5
1.2
1.8
0.9
2.5
1.7
0.8
2.8
2.9
1.2
3.2
2.4
CTRL
HA200
HA500
Sr2HA200
Sr2HA500
Sr4HA200
Sr4HA500
SrCl2
SrCl2
SrCl2
SrCl2

Figure 7.

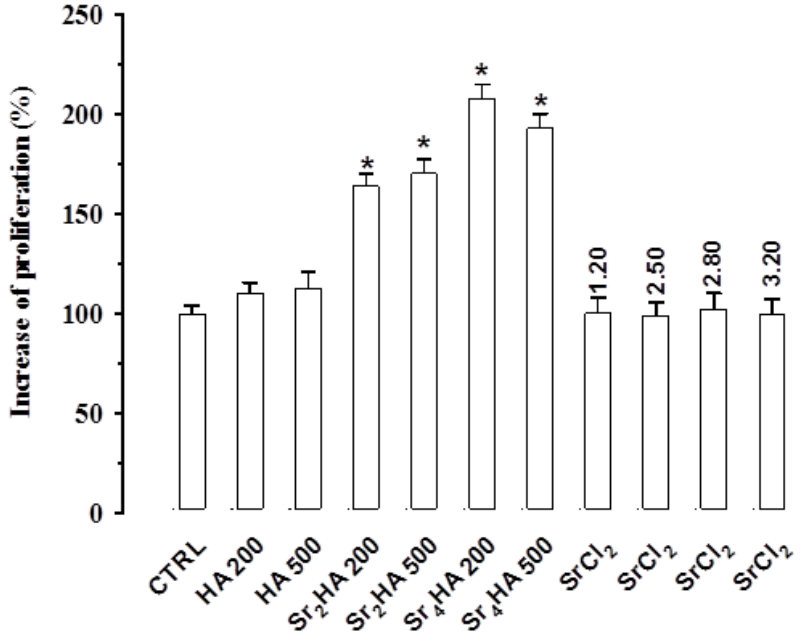
Increase of proliferation (%)
250
200
150
100
50
0
*
*
*
*
1.20
2.50
2.80
3.20
CTRL
HA 200
HA 500
Sr2HA 200
Sr2HA 500
Sr4HA 200
Sr4HA 500
SrCl2
SrCl2
SrCl2
SrCl2

Figure 8.

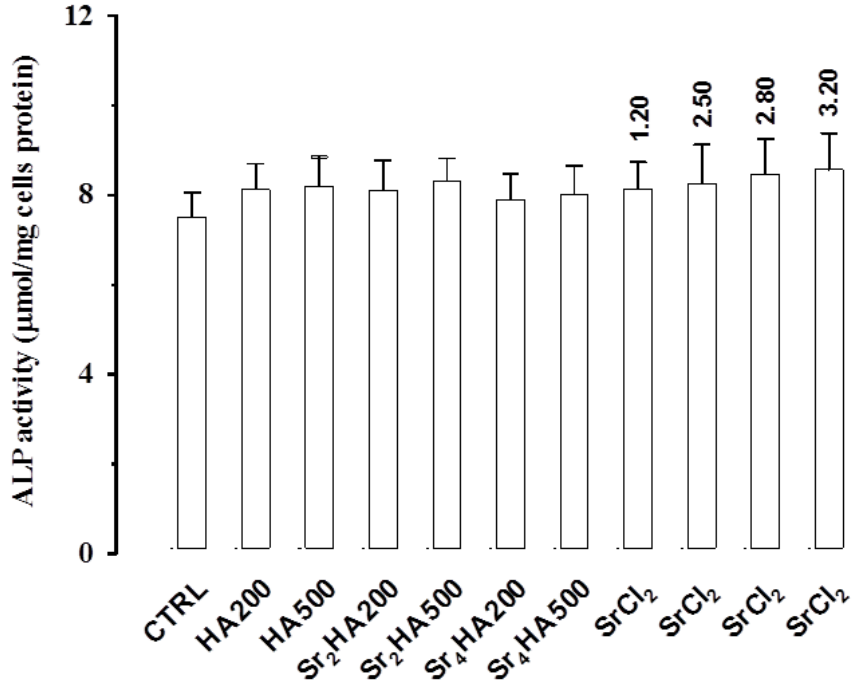
ALP activity (µmol/mg cells protein)
12
8
4
0
1.20
2.50
2.80
3.20
CTRL
HA200
HA500
Sr2HA200
Sr2HA500
Sr4HA200
Sr4HA500
SrCl2
SrCl2
SrCl2
SrCl2

Tables.

Table 1. Summary of the synthesis methods reported in the literature for Sr-substituted HA and the achieved products.

Synthesis method	Substituted ion	Products
Aqueous precipitation to give HA + carbonated HA (cHA), then ion exchange.	Mg^{2+}, Sr^{2+}	Non-stoichiometric apatites: HA: Ca/(P) ratio = 1.46; cHA 1.41 [8]
Aqueous neutralization.	Sr^{2+}	Poorly crystalline HA; pure Sr-substituted apatite after heat treatment at 1250˚C. (Sr+Ca)/P ratio = 1.66 maintained through heat treatment [6]
Wet chemical route.	Mg^{2+}, Sr^{2+}	Poorly crystalline apatite; transformation to β-TCP at 800˚C [starting (Ca+Sr+Mg)/P molar ratio = 1.5] [10]
Aqueous precipitation.	Sr^{2+}	α-TCP after heat-treatment at 1500˚C [19]
Aqueous precipitation.	Mg^{2+}, Sr^{2+}	Sr-substituted: 100% α-TCP; Mg-substituted: 84.6% α-TCP , 15.4% β-TCP [11]
Aqueous precipitation.	Sr^{2+}	Precipitates dried at 110˚C – varying inhomogeneity; after heating at 950˚C, more crystalline, solid solution between CaHA and SrHA [20]
Aqueous precipitation.	Sr^{2+}, Cu^{2+}	HA solid solutions, (Ca+Sr+Cu)/P = 1.666 [21]
Aqueous precipitation.	Sr^{2+}	Sr-substituted HA. 15% substitution: (0 0 2) peak broadened and shifted to smaller angle, and reduced crystallinity for this material [5]
Aqueous precipitation.	Sr^{2+}	HA (Sr-substituted, $(Sr_xCa_{1-x})_5(PO_4)_3OH$ x=0-0.25-0.50-0.75-1.00). Synthesis under 90°C, crystallite size decrease with up to 25% substitution of Sr then increased with higher content [36]
Hydrothermal.	Sr^{2+}	Crystalline, homogeneous solid solutions (of Sr-substituted HA) [15]
Hydrothermal.	Sr^{2+}	Sr- substituted HA: very like HA [16]
Hydrothermal.	Sr^{2+}	HA (Sr-substituted) [17]
Hydrothermal	Cd^{2+}, Sr^{2+}, Pb^{2+}	Pure apatite phase, independent of molar ratio. In general, addition of M up to M/(M+Ca) decreased crystallinity. [18]
Ion exchange.	Sr^{2+}	(Ca+Sr)/(P+C) = 1.67 [6]
Ion-exchange (immersion in aqueous solution of substituent ions with cyclic pH variation).	Mg^{2+}, Sr^{2+}	Different phases obtained from different ion concentrations in solutions and heat treatments at different temperatures. Mg^{2+}: HA, β-TCP, $MgNH_4PO_4$, Mg-β-TCP, $Mg_2P_2O_7$, $MgCaP_2O_7$; Sr^{2+}: HA, Sr-substituted HA, Sr-substituted β-TCP, β-TCP. [51]
Solid state.	Sr^{2+}	SrHA less crystalline. Ca_7Sr_3HA and Ca_6Sr_4HA – unrecognizable diffraction patterns. Others: more like that of SrHA. [22]

Table 2. Number of moles of reactants used and metal/phosphorus molar ratios in the solid-state synthesis of strontium substituted hydroxyapatite.

Desired composition	No. of moles of reactants used			M/P molar ratio (M = Ca+ Sr)
	$CaHPO_4$	$CaCO_3$	$SrCO_3$	
$Ca_{10}(PO_4)_6(OH)_2$	0.06	0.04	-	1.67
$Ca_8Sr_2(PO_4)_6(OH)_2$	0.06	0.02	0.02	1.67
$Ca_6Sr_4(PO_4)_6(OH)_2$	0.06	-	0.04	1.67

Table 3. Data obtained by XRPD analysis.

Nominal composition	(*h k l*)	Intensity [counts]	d [Å]	Position [°2θ]	FWHM [°2θ]	a=b[Å]	c[Å]	Crystallite size *d* [Å]	Crystallinity degree (*Xc*) [%± 4]
$Ca_{10}(PO_4)_6(OH)_2$	(2 1 1)	25611	2.81	31.84	0.10	9.413(3)	6.879(5)	817±25	93
	(0 0 2)	8888	3.44	25.93					
	(3 0 0)	14533	2.72	32.97					
$Ca_8Sr_2(PO_4)_6(OH)_2$	(2 1 1)	13376	2.84	31.51	0.13	9.486(1)	6.959(2)	629±15	87
	(0 0 2)	3885	3.48	25.57					
	(3 0 0)	7258	2.74	32.67					
$Ca_6Sr_4(PO_4)_6(OH)_2$	(2 1 1)	12594	2.87	31.19	0.23	9.546(4)	7.029(3)	354±10	84
	(0 0 2)	3410	3.53	25.23					
	(3 0 0)	6454	2.77	32.37					

Table 4. Measured specific surface areas of materials.

Sample	BET specific surface area [m^2/g]
$Ca_{10}(PO_4)_6(OH)_2$	1.2 ± 0.1
$Ca_8Sr_2(PO_4)_6(OH)_2$	1.1 ± 0.1
$Ca_6Sr_4(PO_4)_6(OH)_2$	0.6 ± 0.1

Table 5. Part A: XPS elemental analysis for the studied materials. Data are reported as atomic % (at %) and given values are the average of measurements taken over three different locations on the samples. In parentheses are reported the data obtained considering, only the elements O, Ca, Sr and P (neglecting C). **Part B**: ESEM-EDS analysis for the studied samples. Given values are the average of measurements taken over 2 different samples of the same nominal composition, on which the EDS analysis was performed over four different areas.

Samples	**A**					
	Element / at % ± SE					
	O	**Ca**	**C**	**Sr**	**Ca + Sr**	**P**
$Ca_{10}(PO_4)_6(OH)_2$	19.2 ±5 (73.0)	4.1 ±1 (15.6)	71.1±5	-	4.1 ±1 (15.6)	3.0 ±1 (11.4)
$Ca_8Sr_2(PO_4)_6(OH)_2$	26.6 ±5 (66.3)	6.6 ±1 (16.5)	59.9±5	1.0 ±1 (2.5)	7.6 ±1 (19.0)	4.6 ±1 (11.5)
$Ca_6Sr_4(PO_4)_6(OH)_2$	36.7±5 (61.8)	7.2 ±1 (12.1)	40.6±5	5.7 ±1 (9.6)	12.9 ±1 (21.7)	9.9 ±1 (16.7)
	B					
	Element / at % ± SE					
	O	**Ca**		**Sr**		**P**
$Ca_{10}(PO_4)_6(OH)_2$	62±5	23±5		-		15±2
$Ca_8Sr_2(PO_4)_6(OH)_2$	66±5	17±3		4.0±0.5		12±2
$Ca_6Sr_4(PO_4)_6(OH)_2$	62±7	15±5		10±2		14±2

Nominal Composition: $Ca_{10}(PO_4)_6(OH)_2$ (O=61.9, Ca=23.8, P=14.4); $Ca_8Sr_2(PO_4)_6(OH)_2$ (O=61.9, Ca=19.0, Sr=4.8, P=14.3); $Ca_6Sr_4(PO_4)_6(OH)_2$ (O=61.9, Ca=14.3, Sr=9.5, P=14.3).

Table 6. Molar ratios calculated from XPS and EDS elemental analysis are reported *vs* theoretical ratios. The values determined by EDS analysis are reported in parentheses.

Sample	**M/P ratio (M = Ca+Sr)**	**Sr/Ca ratio**	**Ca/P ratio**	**Sr/P ratio**
		Measured XPS (EDS) / Theoretical (T)		
$Ca_{10}(PO_4)_6(OH)_2$	**1.37 (1.53)** / 1.67	**- (-)** / -	**1.37 (1.53)** / 1.67	**- (-)** / -
$Ca_8Sr_2(PO_4)_6(OH)_2$	**1.65 (1.75)** / 1.67	**0.15 (0.24)** / 0.25	**1.43 (1.42)** / 1.33	**0.22 (0.22)** / 0.33
$Ca_6Sr_4(PO_4)_6(OH)_2$	**1.30 (1.79)** / 1.67	**0.79 (0.67)** / 0.67	**0.73 (1.07)** / 1.00	**0.60 (0.57)** / 0.66

Table 7. Concentration (ppm) of released ions in MEM, after different times of soaking of samples at two different concentrations (200 μg/ml and 500 μg/ml). Concentrations are also reported using units of μM, with values in parentheses.

Samples / Reaction Times	Ca (ppm ± 0.5)	Sr (ppm ± 0.3)	PO_4 (ppm ± 0.4)
$Ca_{10}(PO_4)_6(OH)_2$			
at 200 μg/ml			
1 day	2.7 (67 μM)	/	0.9 (29.1 μM)
7 days	3.8 (95 μM)	/	2.1 (68 μM)
14 days	3.9 (97.5 μM)	/	2.5 (81 μM)
at 500 μg/ml			
1 day	7.7 (192.5 μM)	/	2.4 (78 μM)
7 days	9.8 (245 μM)	/	3.5 (113 μM)
14 days	4.6 (115 μM)	/	1.9 (61 μM)
$Ca_8Sr_2(PO_4)_6(OH)_2$			
at 200 μg/ml			
1 day	1.2 (30 μM)	0.5 (5.7 μM)	1.1 (36 μM)
7 days	2.7 (67 μM)	1.2 (13.7 μM)	1.8 (58 μM)
14 days	3.5 (87.5 μM)	1.8 (20.5 μM)	2.4 (78 μM)
at 500 μg/ml			
1 day	4.2 (105 μM)	0.9 (10.3 μM)	1.4 (45 μM)
7 days	8.7 (217.5 μM)	2.5 (28.5 μM)	2.9 (94 μM)
14 days	4.8 (120 μM)	1.7 (19.4 μM)	/ (0 μM)
$Ca_6Sr_4(PO_4)_6(OH)_2$			
at 200 μg/ml			
1 day	1.0 (25 μM)	0.8 (9.1 μM)	0.6 (19 μM)
7 days	2.1 (52.5 μM)	2.8 (31.2 μM)	1.4 (43 μM)
14 days	2.9 (72.5 μM)	2.9 (33.1 μM)	2.0 (65 μM)
at 500 μg/ml			
1 day	2.8 (70 μM)	1.2 (13.7 μM)	0.8 (26 μM)
7 days	5.6 (140 μM)	3.2 (36.5 μM)	2.4 (78 μM)
14 days	5.2 (130 μM)	2.4 (27.3 μM)	0.9 (29 μM)

Acknowledgements

This work was financially supported by the Italian Ministry MUR (Project COFIN-2006, Prot. 2006032335_004: “Interface phenomena in silica-based nanostructured biocompatible materials contacted with biological systems”) and by Compagnia San Paolo (Project ORTO11RRT5).

V.A. kindly acknowledges Regione Piemonte, Italy, for a postdoctoral fellowship. F.E.I. acknowledges the ERASMUS programme for financial support during her research study at the University of Torino.

The authors thank Prof. G. Martra, Prof. C. Morterra and Prof. S. Coluccia of the University of Torino, Prof. L. Menabue of the University of Modena and Reggio Emilia for the fruitful discussions.

The authors thank Prof. C. Bianchi of the University of Milano for XPS measurements.

References

[1] L.J. Shyu, L. Perez, S. ZAwacki, J.C. Heughebaert, G.H. Nancollas, J. Dental Res. 62 (1983) 398-352.

[2] Z. Evis, T.J. Webster, Advances in Appl. Ceramics 110 (2011) 311-320.

[3] M. Matos, J. Terra, D.E. Ellis, J. of Physics-Condensed Matter 22 (2010) 145502-145512.

[4] M. Wakamura, K. Kandori, T. Ishikawa, Colloids and Surfaces A Physico-chemical and Eng. Aspects 164 (2000) 297-305.

[5] Z.Y. Li, W.M. Lam, C. Yang, B. Xu, G.X. Ni, S.A. Abbah, K.M.C. Cheung, K.D.K. Luk, W.W. Lu. Biomaterials 28 (2007) 1452-1460.

[6] E. Landi, A. Tampieri, G. Celotti, S. Sprio, M. Sandri, G. Logroscino, Acta Biomaterialia 3 (2007) 961-969.

[7] J. Christoffersen, M.R. Christoffersen, N. Kolthoff, O. Barenholdt, Bone 20 (1997) 47-54.

[8] C. Drouet, M.T. Carayon, C. Combes, C. Rey, Mat. Science and Eng. C- Biomimetic and Supramolecular Systems 28 (2008) 1544-1550.

[9] W.M. Lam, H.B. Pan, Z.Y. Li, C. Yang, W.K. Chan, C.T. Wong, K.D.K. Luk, W.W. Lu. Ceramics International 36 (2010) 683-688.

[10] S. Kannan, F. Goetz-Neunhoeffer, J. Neubauer, S. Pina, P.M.C. Torres, J.M.F. Ferreira, Acta Biomaterialia 6 (2010) 571-576.

[11] S. Pina, P.M.C. Torres, J.M.F. Ferreira. J. of Materials Science-Materials in Medicine 21 (2010) 431-438.

[12] E. Boanini, P. Torricelli, M. Fini, A. Bigi, J. of Materials Science-Materials in Medicine 22 (2011) 2079-2088.

[13] M. Roy, A. Bandyopadhyay, S. Bose, J. of Biomedical Materials Research Part B-Applied Biomaterials 99B (2011) 258-265.

[14] C. Capuccini, P. Torricelli, F. Sima, E. Boanini, C. Ristoscu, B. Bracci, G. Socol, M. Fini, I.N. Mihailescu, A..Bigi, Acta Biomaterialia 4 (2008) 1885-1893.

[15] H.P. Schoenberg. Biochimica et Biophysica Acta 75 (1963) 96-102.

[16] M. Kikuchi, A. Yamazaki, R. Otsuka, M. Akao, Aoki H. J. of Solid State Chemistry 113 (1994) 373-378.

[17] B. Donazzon, G. Dechambre, J.L. Lacout. Annales De Chimie-Science Des Materiaux 23 (1998) 53-58.

[18] K. Yanagisawa, K. Zhu, T. Fujino, A. Onda, K. Kajiyoshi, K. Ioku, Bioceramics 18, 309 (2006) 57-60.

[19] S. Pina, P.M. Torres, F. Goetz-Neunhoeffer, J. Neubauer, J.M.F. Ferreira. Acta Biomaterialia 6 (2010) 928-935.

[20] R.L. Collin, J. of the Am. Chem. Society 81 (1959) 5275-5281.

[21] M. Pujari, P.N. Patel. J. of Solid State Chemistry 83 (1989) 100-104.

[22] C. Lagergren, D. Carlstrom C Acta Chemica Scandinavica 11 (1957) 545-550.

[23] J. Zeglinski, M. Nolan, M. Bredol, A. Schattec, S.A.M. Tofail. Phys. Chem. Chem. Phys., 14 (2012) 3435-3443.

[24] V. Aina, A. Perardi, L. Bergandi, G. Malavasi, L. Menabue, C. Morterra, D. Ghigo, Chemico-Biological Interactions 167 (2007) 207-218.

[25] H. Klug, L. Alexander X-Ray Diffraction Procedures. New York, 1962.

[26] E. Landi, A. Tampieri, G. Celotti, S. Sprio J. of the European Ceramic Society 20 (2000) 2377-2387.

[27] A.C. Larson, R.B. Von Dreele, General structure analysis system (GSAS), 1994.

[28] B.H. Toby, J. Appl. Crystallogr. 34 (2001) 210-213.

[29] K. Sudarsanan, R.A. Young, Acta Crystallogr. B 25 (1969) 1534-1538.

[30] V. Aina, F. Bonino, C. Morterra, M. Miola, C.L. Bianchi, G. Malavasi, M. Marchetti, V. Bolis, J. of Phys.Chemistry C 115 (2011) 2196-2210.

[31] V. Aina, G. Magnacca, G. Cerrato, F. Bonino, G. Malavasi, C. Morterra Nuovo Cimento Della Societa Italiana Di Fisica B-General Physics Relativity Astronomy and Mathematical Physics and Methods 123 (2008) 1517-1528.

[32] S. Brunauer, P.H. Emmet, E.J.Teller J. Am. Chem. Soc. 60 (1938) 309-312.

[33] T. Kokubo, H.Takadama Biomaterials 27 (2006) 2907-2915.

[34] G. Lusvardi, G. Malavasi, L. Menabue, V. Aina, C. Morterra, Acta Biomaterialia 5 (2009) 3548-3562.

[35] A. Pollack, C.B. Bagwell, G.L. Irvin. Science 203 (1979) 1025-1029.

[36] M.D. O'Donnell, Y. Fredholm, A. de Rouffignac, R.G. Hill, Acta Biomaterialia 4 (2008) 1455-1457.

[37] R.D. Shannon, C.T. Prewitt, Acta Crystallogr. B 25 (1969)785-790.

[38] J. Kolmas, A. Jaklewicz, A. Zima, M. Bucko, Z. Paszkiewicz, J. Lis, A. Slósarczyk, W. Kolodziejski, J. of Molecular Structure 987 (2011) 40-48.

[39] V. Aina, C. Morterra, G. Lusvardi, G. Malavasi, L. Menabue, S. Shruti, C.L. Bianchi, V. Bolis, J. of Physical Chemistry C 115 (2011) 22461-22474.

[40] G. Penel, G. Leroy, C. Rey, E. Bres Calcif. Tissue Int. 63 (1998) 475-481.

[41] G.X. Ni, Z.P. Yao, G.T. Huang, W.G. Liu, W.W. Lu, J. of Materials Science-Materials in Medicine 22 (2011) 961-967.

[42] S. Peng, X.S. Liu, S. Huang, Z. Li, H. Pan, W. Zhen, K.D.K. Luk, X.E. Guo, W.W. Lu, Bone 49 (2011) 1290-1298.

[43] J. Braux, F. Velard, C. Guillaume, S. Bouthors, E. Jallot, J.M. Nedelec, D. Laurent-Maquin, P. Laquerriere, Acta Biomaterialia 7 (2011) 2593-2603.

[44] S. Pina, S.I. Vieira, P. Rego, P.M.C. Torres, O.A.B. da Cruz e Silva, E.F. da Cruz e Silva, J.M.F. Ferreira, European Cells and Materials 20 (2010) 162-177.

[45] J.W. Park, Y.J. Kim, J.H. Jang. Clinical Oral Implants Research 21 (2010) 398-406.

[46] E. Bonnelye, A. Chabadel, F. Saltel, P. Bone 42 (2008) 129-138.

[47] E. Canalis, M. Hott, P. Deloffre, Y. Tsouderos, P.J. Marie. Bone 18 (1996) 517-523.

[48] J. Caverzasio Bone 42 (2008) 1131-1136.

[49] E. Gentleman, Y.C. Fredholm, G. Jell, N. Lotfibakhshaiesh, M.D. O'Donnell, R.G. Hill, M.M. Stevens. Biomaterials 31 (2010) 3949-3956.

[50] M.D. O'Donnell, P.L. Candarlioglu, C.A. Miller, E. Gentleman, M.M. Stevens, J. of Materials Chemistry 20 (2010) 8934-8941.

[51] A. Bigi, F. Marchetti, A. Ripamonti, N. Roveri, E. Foresti J. of Inorganic biochemistry 15 (1981) 317-321.